

# Transferability of crystal-field parameters for rare-earth ions in $\text{Y}_2\text{SiO}_5$ tested by Zeeman spectroscopy

N. L. Jobbitt<sup>a,b</sup>, S. J. Patchett<sup>a,b</sup>, Y. Alizadeh<sup>a,b</sup>, M. F. Reid<sup>a,b,\*</sup>,  
J.-P. R. Wells<sup>a,b</sup>, S. P. Horvath<sup>a,c</sup>, J. J. Longdell<sup>b,c</sup>,  
A. Ferrier<sup>d,e</sup> and P. Goldner<sup>d</sup>

<sup>a</sup>School of Physical and Chemical Sciences, University of Canterbury,  
PB 4800, Christchurch 8140, New Zealand

<sup>b</sup>The Dodd-Walls Centre for Photonic and Quantum Technologies,  
New Zealand

<sup>c</sup>Department of Physics, University of Otago, PB 56, Dunedin,  
New Zealand

<sup>d</sup>Chimie ParisTech, PSL University, CNRS,  
Institut de Recherche de Chimie Paris, Paris, France

<sup>e</sup>Faculté des Sciences et Ingénierie, Sorbonne Université, Paris, France

\*Email: [mike.reid@canterbury.ac.nz](mailto:mike.reid@canterbury.ac.nz)

November 2, 2018

**Abstract**— Zeeman spectroscopy is used to demonstrate that phenomenological crystal-field parameters determined for the two  $C_1$  point-group sites in  $\text{Er}^{3+}:\text{Y}_2\text{SiO}_5$  may be transferred to other ions. The two crystallographic six- and seven-coordinate substitutional sites may be distinguished by comparing the spectra with crystal-field calculations.

# 1 Introduction

Yttrium orthosilicate ( $\text{Y}_2\text{SiO}_5$ ) doped with rare-earth ions has been widely used over the past decade in the development of quantum-information devices. Yttrium has a very small nuclear magnetic moment, while isotopes of Si and O with non-zero nuclear spin have very low natural abundances. This minimises decoherence due to spin flips, giving outstanding coherence properties. Furthermore, the rare-earth substitutional sites in  $\text{Y}_2\text{SiO}_5$  has  $C_1$  point-group symmetry, giving highly admixed wavefunctions and enabling efficient and diverse optical pumping schemes [1, 2, 3].

Performance improvements for these devices rely on accurate modelling of magnetic-hyperfine structure. For example, the spin Hamiltonian for  $\text{Eu}^{3+}:\text{Y}_2\text{SiO}_5$  was utilized in a computational search for magnetic field orientations exhibiting a near-zero gradient with respect to hyperfine energy levels. This Zero-First-Order-Zeeman (ZEFOZ) technique enabled an experimental demonstration of a coherence time of six hours in  $^{151}\text{Eu}^{3+}:\text{Y}_2\text{SiO}_5$  [4].

Spin Hamiltonians are not transferable between electronic levels of the same ion, or to other ions. This limits the opportunity to explore candidate systems by theoretical modelling. On the other hand, crystal-field calculations [5, 6, 7, 8] model the electronic structure of the entire  $4f^N$  configuration. The parameters show systematic trends across the rare-earth series, so they may be transferred from ion to ion. Crystal-field calculations may be used to construct spin Hamiltonians, or used directly for magnetic-hyperfine calculations. Since the crystal-field Hamiltonian automatically handles mixing of crystal-field levels by a magnetic field, crystal-field calculations may be used to extend the ZEFOZ method to large magnetic fields where a simple spin Hamiltonian approach breaks down. This is particularly relevant given the demonstration of a coherence time exceeding one second in  $\text{Er}^{3+}:\text{Y}_2\text{SiO}_5$  using a 7 Tesla magnetic field by Rančić et al. [9].

Determination of crystal-field parameters for low-symmetry systems is non-trivial. Data from Zeeman splitting is essential to give orientation information necessary to determine a unique set of parameters [10, 11]. In  $C_1$  symmetry (i.e. no symmetry) there are 27 crystal-field parameters, which makes calculations computationally challenging. Previous work on  $C_1$  symmetry sites has been based on *ab initio* calculations [12, 13, 14], or the use of a higher-symmetry approximation to reduce the number of parameters [15, 16].

We have recently developed techniques that make full phenomenological crystal-field fits for  $C_1$  point-group symmetry sites practical. These methods have been applied to both sites of  $\text{Er}^{3+}:\text{Y}_2\text{SiO}_5$  [17, 18]. The fits used both optical, magneto-optical and electron-paramagnetic resonance experimental data from the literature [13, 19, 20].

In this work we demonstrate the transferability of the crystal-field parameters to the ions  $\text{Sm}^{3+}$  and  $\text{Nd}^{3+}$  by performing Zeeman spectroscopy. Calculations based on the  $\text{Er}^{3+}$  parameters clearly distinguish the two sites, and this information may be combined with EPR and ab-initio calculations for particular ions to allow the identification of sites.

## 2 Experimental and theoretical techniques

$\text{Y}_2\text{SiO}_5$  (in the X2 phase) is a monoclinic crystal with  $C_{2h}^6$  space group symmetry. The yttrium ions occupy two crystallographically distinct sites, each with  $C_1$  point-group symmetry, referred to as site 1 and site 2, corresponding to oxygen coordination numbers of six and seven, respectively [21].  $\text{Y}_2\text{SiO}_5$  has three perpendicular optical-extinction axes: the crystallographic  $b$  axis, and two mutually perpendicular axes labelled  $D_1$  and  $D_2$ . In our calculations we follow the convention of identifying these as the  $z$ ,  $x$ , and  $y$  axes respectively [19].

Samples of  $\text{Y}_2\text{SiO}_5$  doped with  $\text{Er}^{3+}$  (50 ppm) and  $\text{Nd}^{3+}$  (200 ppm) were prepared in Paris. The  $\text{Sm}^{3+}$  (5000 ppm) sample was supplied by Scientific Materials. All samples were oriented using Laue backscattering. The samples were cuboids with the  $D_1$  and  $D_2$  and  $b$  axes through the faces and dimensions of approximately 5 mm. Infrared spectroscopy was performed using a  $0.075\text{ cm}^{-1}$  resolution Bruker Vertex 80 with an optical path purged by  $\text{N}_2$  gas. Zeeman spectroscopy was performed using a 4 T, simple solenoid, superconducting magnet with samples cooled by thermal contact with a copper sample holder fixed through the centre of the solenoid. Measurements were carried out at 4.2 K.

The Hamiltonian appropriate for modelling the  $4f^N$  configuration is [5, 6, 8]

$$H = H_{\text{FI}} + H_{\text{CF}} + H_{\text{Z}} + H_{\text{HF}}. \quad (1)$$

The terms in this equation represent the free-ion contribution, the crystal-field interaction, the Zeeman term, and the electron-nuclear hyperfine interaction.

The free-ion Hamiltonian may be written as

$$\begin{aligned}
H_{\text{FI}} = & E_{\text{avg}} + \sum_{k=2,4,6} F^k f_k + \zeta A_{\text{SO}} + \alpha L(L+1) + \gamma G(R_7) \\
& + \beta G(G_2) + \sum_{i=2,3,4,6,7,8} T^i t_i + \sum_{i=0,2,4} M^i m_i + \sum_{i=2,4,6} P^i p_i. \quad (2)
\end{aligned}$$

$E_{\text{avg}}$  is a constant configurational shift,  $F^k$  Slater parameters characterizing aspherical electrostatic repulsion, and  $\zeta$  the spin-orbit coupling constant. The other terms parametrize two- and three- body interactions, as well as higher-order spin-dependent effects [5, 8].

The crystal-field Hamiltonian has the form

$$H_{\text{CF}} = \sum_{k,q} B_q^k C_q^{(k)}, \quad (3)$$

for  $k = 2, 4, 6$  and  $q = -k \dots k$ . The  $B_q^k$  parameters are the crystal-field expansion coefficients and  $C_q^{(k)}$  are spherical tensor operators. In  $C_1$  symmetry all non-axial ( $q \neq 0$ )  $B_q^k$  parameters are complex, leading to a total of 27 parameters.

We do not explicitly consider hyperfine interactions in this work. The reader is referred to Refs. [17, 11, 18] for a discussion of the calculation of hyperfine effects with a crystal-field model.

The Zeeman interaction for an external magnetic field is represented by

$$H_Z = \mu_B \mathbf{B} \cdot (\mathbf{L} + 2\mathbf{S}), \quad (4)$$

where  $\mu_B$  is the Bohr magneton, and  $\mathbf{L}$  and  $\mathbf{S}$  are the total orbital and spin angular momenta. In this work we only consider Kramers ions (with total spin a multiple of  $\hbar/2$ ). For Kramers ions in low-symmetry sites all electronic levels are doubly-degenerate in the absence of an applied magnetic field. For low magnetic fields the splitting of these doublets may be parametrized by  $g$  values, such that the splitting  $\Delta_E$  is a function of the magnetic field  $\mathbf{B}$  applied in a particular direction:

$$\Delta_E = g\mu_B |\mathbf{B}|. \quad (5)$$

Transitions between the ground electronic state and an excited electronic state will, in general, contain four spectral lines, as indicated schematically in Figure 1, with the energy differences depending on sums and differences

of ground and excited-state  $g$  values. Measurements of these differences can reveal a large amount of information regarding the wavefunctions and the effect of magnetic fields using moderately high-resolution spectroscopy, such as Fourier-transform absorption spectroscopy. In contrast, non-Kramers ions in low-symmetry sites have no electronic degeneracy and measurements of magnetic splitting of the hyperfine structure usually requires high-resolution techniques, such as in Ref. [4].

Parameters for Site 1 and Site 2 of  $\text{Er}^{3+}:\text{Y}_2\text{SiO}_5$  (using the convention of Ref. [19]) are given by Horvath [17]. An alternative parameter set for Site 1 is given in Ref. [18]. However, since the latter is optimised for high-resolution magneto-hyperfine data, we use the former in this work, as this gives more consistency between the parameter sets for the two sites. Since the ionic radius and the crystal-field parameters reduce across the rare-earth series [5, 6, 7, 8], the crystal-field parameters for  $\text{Sm}^{3+}$  and  $\text{Nd}^{3+}$  should be scaled up from the  $\text{Er}^{3+}$  parameters. However we found that for the levels considered here, scaling made a very small difference, and the calculations presented here use unscaled parameters. The free-ion parameters for  $\text{Sm}^{3+}$  and  $\text{Nd}^{3+}$  were taken from Ref. [5].

### 3 Results and discussion

Zeeman spectra for  $\text{Nd}^{3+}$ ,  $\text{Sm}^{3+}$ , and  $\text{Er}^{3+}$  in  $\text{Y}_2\text{SiO}_5$  crystals are given in Figure 2. Calculated magnetic splittings for the particular orientation and field chosen are indicated on the diagrams. Details of the transitions and magnetic fields are given in Table 1, along with calculated  $g$  values.

#### 3.1 $\text{Er}^{3+}:\text{Y}_2\text{SiO}_5$

We begin with  $\text{Er}^{3+}:\text{Y}_2\text{SiO}_5$ , since this is the ion for which the crystal-field parameters were determined [17, 18].  $\text{Er}^{3+}$  has 11  $4f$  electrons and has a relatively small ionic radius, similar to  $\text{Y}^{3+}$ , so it would be expected to substitute equally into both  $\text{Y}^{3+}$  sites.

Figure 2(c) shows the spectrum of  $\text{Er}^{3+}:\text{Y}_2\text{SiO}_5$  in the region of the transitions from the ground state to the lowest-energy  ${}^4\text{I}_{13/2}$  states for each site, with a 1 T field along the  $b$  axis. The magnetic splittings of these transitions were extensively studied by Sun et al. [19] and our spectrum corresponds to the  $\theta = 0$  points of their Figures 3(c) and 4(c). The data from that

study was crucial input to the crystal-field fit [17, 18]. The magnetic splittings of other transitions are also generally in good agreement, confirming the experimental energy-level assignments used in the fits.

The absorption for the Site 1 and Site 2 transitions is comparable, so if the oscillator strengths are assumed to be similar then the concentration of  $\text{Er}^{3+}$  in each site is comparable. The crystal-field splitting for Site 1 is larger than for Site 2 [13], and this is reflected in our fitted crystal-field parameters [17]. This suggests that Site 1 is the six-fold coordinate site, for which the crystal-field parameters are calculated to be larger [14].

### 3.2 $\text{Nd}^{3+}:\text{Y}_2\text{SiO}_5$

$\text{Nd}^{3+}$  has 3  $4f$  electrons, so has a larger ionic radius than  $\text{Er}^{3+}$  and substitution into the seven-coordinate site is expected to be favoured. The site with the largest absorbance, labelled Type 1 in Ref. [22], has been studied by EPR [23, 16]. In Ref. [16] this site was identified as seven-coordinate by pulsed EPR measurements.

Figure 2(a) shows the spectrum of  $\text{Nd}^{3+}:\text{Y}_2\text{SiO}_5$  in the region of the transitions from the ground state to the lowest-energy  ${}^4\text{F}_{3/2}$  states for each site, with a 2 T field along the  $b$  axis. The magnetic splitting for the site with the strongest absorption matches the Site 2 calculation. The spectrum, and the calculated ground-state  $g$  value of 4 for a field along the  $b$  axis is consistent with the EPR data.

### 3.3 $\text{Sm}^{3+}:\text{Y}_2\text{SiO}_5$

$\text{Sm}^{3+}$  is a Kramers ion with a large number of absorption lines in the IR, visible, and UV spectral regions. It is, therefore, an ideal ion for extensive Zeeman measurements.

$\text{Sm}^{3+}$  has 5  $4f$  electrons, so it has an ionic radius slightly smaller than  $\text{Nd}^{3+}$  and, again, substitution into the seven-coordinate site is expected to be favoured. Figure 2(b) shows the spectrum of  $\text{Sm}^{3+}:\text{Y}_2\text{SiO}_5$  in the region of the transitions from the ground state to the lowest-energy  ${}^6\text{H}_{13/2}$  states for each site, with a 4 T field along the  $D_1$  axis.

The magnetic splitting for the transitions with highest absorbance is consistent with the Site 2 calculation. The  $g$  values for the ground state for both sites are small (Table 1) and are not fully resolved in Figure 2(b), whereas the excited-state  $g$  values are large, particularly for Site 2.

## 4 Conclusions

We have used Zeeman spectroscopy to demonstrate that crystal-field parameters determined for  $\text{Er}^{3+}$  in the two  $\text{Y}_2\text{SiO}_5$  substitutional sites give a reasonable account of magnetic splittings in other ions. Future work will use more extensive measurements to refine the crystal-field parameters across the rare-earth series. This will provide improved modelling relevant to the development of quantum-information applications.

## References

- [1] L. Rippe, M. Nilsson, S. Kröll, R. Klieber, and D. Suter. *Physical Review A* **71**, 062328 (2005).
- [2] B. Lauritzen, S. R. Hastings-Simon, H. de Riedmatten, M. Afzelius, and N. Gisin. *Physical Review A* **78**, 043402 (2008).
- [3] J. J. Longdell and M. J. Sellars. *Physical Review A* **69**, 032307 (2004).
- [4] M. Zhong, M. P. Hedges, R. L. Ahlefeldt, J. G. Bartholomew, S. E. Beavan, S. M. Wittig, J. J. Longdell, and M. J. Sellars. *Nature* **517**, 177 (2015).
- [5] W. T. Carnall, G. L. Goodman, K. Rajnak, and R. S. Rana. *The Journal of Chemical Physics* **90**, 3443 (1989).
- [6] C. Görller-Walrand and K. Binnemans. In J. K. A. Gschneidner and L. Eyring, editors, *Handbook on the Physics and Chemistry of Rare Earths*, volume 23, 121, (North-Holland, Amsterdam1996).
- [7] D. J. Newman and B. K. C. Ng, editors. *Crystal Field Handbook*, (Cambridge University Press, Cambridge2000).
- [8] G. Liu. In G. Liu and B. Jacquier, editors, *Spectroscopic Properties of Rare Earths in Optical Materials*, (Springer Science & Business Media2006).
- [9] M. Rančić, M. P. Hedges, R. L. Ahlefeldt, and M. J. Sellars. *Nature Physics* **14**, 50 (2018).

- [10] A. A. Antipin, M. P. Davydova, M. V. Eremin, R. K. Luks, and A. L. Stolov. *Optika i Spektroskopiya* **33**, 673 (1972).
- [11] S. P. Horvath, J.-P. R. Wells, M. F. Reid, M. Yamaga, and M. Honda. Electron paramagnetic resonance enhanced crystal field analysis for low point-group symmetry systems:  $C_{2v}$  sites in  $Sm^{3+}:CaF_2/SrF_2$  (2018). <https://arxiv.org/abs/1809.07397>.
- [12] A. G. Avanesov, V. V. Zhorin, B. Z. Malkin, and V. F. Pisarenko. *Soviet Physics Solid State* (1992).
- [13] J. L. Doualan, C. Labbe, P. L. Boulanger, J. Margerie, R. Moncorge, and H. Timonen. *Journal of Physics: Condensed Matter* **7**, 5111 (1995).
- [14] J. Wen, C.-K. Duan, L. Ning, Y. Huang, S. Zhan, J. Zhang, and M. Yin. *The Journal of Physical Chemistry A* **118**, 4988 (2014).
- [15] O. Guillot-Nol, Y. Le Du, F. Beaudoux, E. Antic-Fidancev, M. F. Reid, R. Marino, J. Lejay, A. Ferrier, and P. Goldner. *Journal of Luminescence* **130**, 1557 (2010).
- [16] A. A. Sukhanov, R. F. Likеров, R. M. Eremina, I. V. Yatsyk, T. P. Gavrilova, V. F. Tarasov, Y. D. Zavartsev, and S. A. Kutovoi. *Journal of Magnetic Resonance* **295**, 12 (2018).
- [17] S. P. Horvath. High-resolution spectroscopy and novel crystal-field methods for rare-earth based quantum information processing. Ph.D. thesis, University of Canterbury (2016). <https://ir.canterbury.ac.nz/handle/10092/12430>.
- [18] S. P. Horvath, J. V. Rakonjac, Y.-H. Chen, J. J. Longdell, P. Goldner, J.-P. R. Wells, and M. F. Reid. A comprehensive understanding of ground and optically-excited hyperfine structure of  $^{167}Er^{3+}:Y_2SiO_5$  (2018). <https://arxiv.org/abs/1809.01058>.
- [19] Y. Sun, T. Böttger, C. W. Thiel, and R. L. Cone. *Physical Review B* **77**, 085124 (2008).
- [20] Y.-H. Chen, X. Fernandez-Gonzalvo, S. P. Horvath, J. V. Rakonjac, and J. J. Longdell. *Physical Review B* **97**, 024419 (2018).



- [21] B. A. Maksimov, V. V. Ilyukhin, Y. A. Khariton, and N. V. Belov. Soviet Physics Crystallography, USSR **15**, 806 (1971).
- [22] R. Beach, M. D. Shinn, L. Davis, R. W. Solarz, and W. F. Krupke. IEEE Journal of Quantum Electronics **26**, 1405 (1990).
- [23] G. Wolfowicz, H. Maier-Flaig, R. Marino, A. Ferrier, H. Vezin, J. J. L. Morton, and P. Goldner. Physical Review Letters **114**, 170503 (2015).

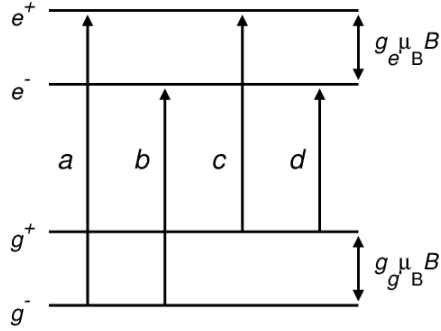


Figure 1: Schematic diagram of Zeeman splitting of ground ( $g^\pm$ ) and excited ( $e^\pm$ ) electronic states of a Kramers ion, and the possible transitions.  $g_g$  and  $g_e$  are the  $g$  values of the ground and excited states.

Table 1: Details of the transitions and magnetic-field settings for the spectra of  $\text{Nd}^{3+}$ ,  $\text{Sm}^{3+}$ , and  $\text{Er}^{3+}$  in  $\text{Y}_2\text{SiO}_5$  given in Figure 2. For each site the experimental wavenumber at zero magnetic field ( $E_0$ ) is listed, and  $g$  values calculated from the crystal-field model, using the notation of Figure 1.

Ion	Excited multiplet	Magnetic Field		Site 1			Site 2		
		axis	$B$ (T)	$E_0$ ( $\text{cm}^{-1}$ )	$g_g$	$g_e$	$E_0$ ( $\text{cm}^{-1}$ )	$g_g$	$g_e$
$\text{Nd}^{3+}$	$^4\text{F}_{3/2}$	$b$	2.0	11309.7	1.20	0.82	11322.5	4.00	0.66
$\text{Sm}^{3+}$	$^6\text{H}_{13/2}$	$D_1$	4.0	4987.8	0.39	6.36	4936.3	0.71	15.00
$\text{Er}^{3+}$	$^4\text{I}_{13/2}$	$b$	1.0	6508.4	7.82	10.00	6498.1	3.04	4.39

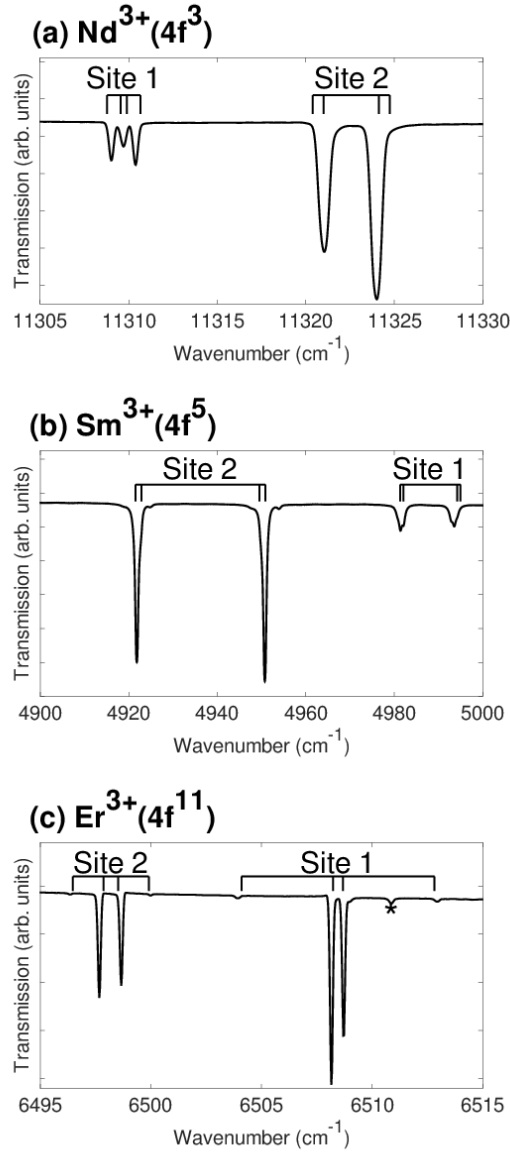


Figure 2: Zeeman spectra for  $Nd^{3+}$ ,  $Sm^{3+}$ , and  $Er^{3+}$  in  $Y_2SiO_5$ . Transitions from the ground state to the lowest-energy states of a particular excited multiplet for each site are shown. Details of the excited multiplets, and the magnetic field directions and strengths, are given in Table 1. Zeeman splittings calculated from the crystal-field model are shown in each plot. All measurements were done at 4.2 K. For  $Sm^{3+}:Y_2SiO_5$ , the small features on the high-energy side of the site 2 lines are satellite lines. For  $Er^{3+}:Y_2SiO_5$ , the feature marked with an asterisk is not associated with  $Er^{3+}$ .